Conflicting effects of a portable ultra-clean airflow unit on the sterility of operating rooms: A numerical investigation

Diego Casagrande, Marzio Piller *

Department of Engineering and Architecture, University of Trieste, Via A. Valerio, 10 - 34127, Trieste (TS), Italy

ARTICLE INFO

Keywords:
Operating room
Bacterial contamination
Instrumentation table
Numerical simulation
Air-cleaner device
Ventilation

ABSTRACT

The onset of post-operatory surgical-site infections is significantly correlated with the concentration of viable airborne bacteria that are shed from the surgical team or entering the operating room during door openings and are deposited directly on the patient's wound or on surgical instruments.

The ultra-clean vertical laminar airflow ventilation system is often used to protect the main surgical area of operating rooms. The clean zone provided by the laminar airflow system is crowded with staff and furniture. As a result, some surgical instruments might remain outside the protected area. We use a numerical simulation to investigate the capability of a portable ultra-clean airflow unit to reduce the contamination of the principal instrumentation table by airborne bacteria, during a sham operation. The numerical model is thoroughly validated against the experimental data available for a test room. The portable air-cleaning device maintains sterile conditions on the principal instrumentation table over a range of flow rates of the general ventilation, although it induces higher levels of bacterial contamination in other zones of the room at the same time.

1. Introduction

Patients in hospital wards have a weakened immune system and are prone to acquire infections, which can be caused either by airborne bacteria, viruses and mold spores or through direct contact with other people or with infected medical equipment and surgical instruments. There is evidence of a strong correlation between the onset of surgical site infections (SSI) and the concentration of airborne bacteria in operating rooms (OR) [1–4]. Skin scales are the primary source of airborne bacteria (also identified as *bacteria carrying particles* (BCPs)), released from both the surgical staff and the patient [5].

Different expedients are commonly used to limit bacterial contamination. Some of these are reducing the permeability of staff clothing, using an efficient ventilation system, and reducing the number and activity of the occupants. A vertical laminar airflow ventilation (LAF) is widely used to protect the surgical area [6–11].

Typically, the clean zone provided by LAF systems is crowded with staff and furniture: hence, some sterile instruments might remain outside the protected area. Movable, laminar airflow units (MLAFs) are relatively compact devices that can be easily repositioned to protect specific areas [12–14]. Using a MLAF unit is a viable option to reduce the contamination of the surgical instrumentation. There exist several types of MLAFs, based on different physical mechanisms: mechanical filtration (portable HEPA screens), ultraviolet germicidal irradiation, volatile organic compounds removal (non-thermal plasma, thermal plasma, biofiltration, high-frequency glow discharge) [15,16]. Nilsson et al. [12] conducted an experimental investigation on the performance of a horizontal LAF instrument table during two sham knee-replacement operations. They conclude that "the instrument table supplied with ultra-clean LAF does increase the cleanliness of the air" and can be safely used in parallel with the main LAF unit. Pasquarella et al. [14] experimentally assessed the efficacy of a movable LAF unit in reducing the bacteria concentration within an operating room endowed with a vertical turbulent ventilation system, during real abdominal surgery operations. The size of the operating theatre is comparable to that of the room investigated in the present work, and the ventilation rate (15 ACH) is the same as considered in one of our test cases. The particle-deposition rate measured for particles less than 0.5μm is comparable to that observed in the present investigation. The authors confirmed the capability of the mobile LAF unit to reduce the bacterial contamination below an acceptable level. von Vogelsang et al. [17] collected a total of 233 samples during 45 neurosurgical operations in operating rooms equipped with conventional turbulent ventilation with additional MLAF units. Using the MLAF units causes a statistically-significant reduction in the bacterial concentration both in the surgical area and above the

* Corresponding author. Dept. of Engineering and Architecture, Università degli Studi di Trieste, Via A. Valerio, 10 - 34127, Trieste (TS), Italy.
E-mail addresses: casagranded@units.it (D. Casagrande), piller@units.it (M. Piller).

Nomenclature abbreviations

ACH	air-changes per hour
BCP	bacteria-carrying particles
CFU	colony-forming unit
CV	control volume
DPM	discrete phase model
DRW	discrete random walk
EIM	eddy interaction model
LAF	laminar airflow
MLAF	mobile laminar airflow
OR	operating room
PDR	particle deposition rate, **BCP/h m^2**
RANS	Reynolds-averaged Navier-Stokes
S2S	surface-to-surface radiation model

Greek letters

α_p	particle load
β_f	thermal expansion coefficient, **K^{-1}**
β_r	extinction coefficient, **km^{-1}**
$\boldsymbol{\tau}$	unit vector tangent to a surface
η	Kolmogorov length scale, $\boldsymbol{\mu}$**m**
λ	mean free path, $\boldsymbol{\mu}$**m**
μ_f	fluid dynamic viscosity, **kg/m s**
ν_f	fluid kinematic viscosity, **m^2/s**
Ω	fluid-particle relative angular velocity, **s^{-1}**
ω_f	fluid angular velocity, **s^{-1}**
ω_p	particle angular velocity, **s^{-1}**
ρ_f	fluid density, **kg/m^3**
ρ_p	particle density, **kg/m^3**
τ	optical thickness, **m**
τ_c	eddy crossing time, **s**
τ_e	eddy lifetime, **s**
τ_i	particle-eddy interaction time, **s**
τ_K	Kolmogorov time scale, **s**
τ_p	particle relaxation time, **s**
ε	rate of dissipation of turbulent kinetic energy, **m^2/ s^3**

Latin letters

$\boldsymbol{n}$	unit vector normal to a surface
a_1, a_2, a_3	drag coefficient constants
C_C	Cunningham (correction) factor
C_D	drag coefficient
C_L	Saffman lift coefficient
C_T	time scale constant
c_{p_f}	specific heat at constant pressure, **J/kg K**
d_p	particle diameter, $\boldsymbol{\mu}$**m**
d_{ij}	rate of deformation tensor, **s^{-1}**
F_B	Basset history force, N
F_D	drag force, N
F_i	inertia force, **N**
F_L	Saffman lift force, **N**
F_M	Magnus lift force, **N**
F_P	pressure gradient force, **N**
F_V	virtual mass force, N
h	heat transfer coefficient, **W/(m^2** K**)**
k	turbulent kinetic energy, **m^2/s^2**
k_f	thermal conductivity, **W/m K**
L_e	eddy length, **m**
L_L	Lagrangian length scale, **m**
L_m	mean beam length, **m**
m_f	fluid mass, **kg**
m_p	particle mass, kg
Re_p	particle Reynolds number
Re_R	rotational Reynolds number
Ri	Richardson number
St_p	particle Stokes number
T_L	Lagrangian integral time scale, **s**
u'	turbulent velocity fluctuation, **m/s**
u_f	fluid velocity, **m/s**
u_p	particle velocity, **m/s**
w^+	updraught velocity, **m/s**
A	area, **m^2**
N	number density, **BCP/m^3**
V	volume, **m^3**

instrumentation table. Sadrizadeh and Holmberg [13] numerically investigated the effect of the MLAF screen velocity on the particle concentration and on the deposition rate on the surgical table and the instrumentation tables in a turbulent-mixing ventilated OR. They highlighted the capability of the ultra-clean mobile airflow unit to keep sterile conditions on the aforementioned targets. Sadrizadeh et al. [18] investigated the influence of the position of the staff members on the performance of the MLAF unit, for a single main-ventilation rate. Friberg

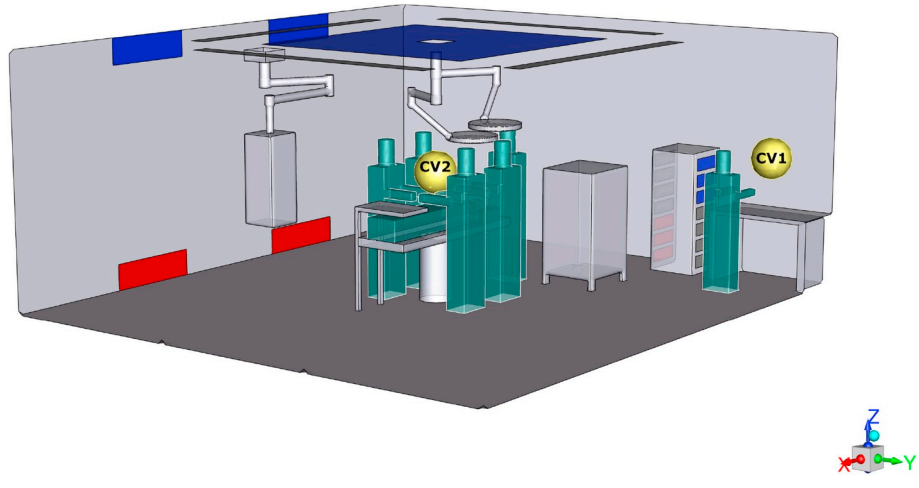

Fig. 1. Sketch of the considered prototype of operating room. The BCP concentration is calculated within the control volumes marked as CV_1 and CV_2.

et al. [19] assessed the interaction of an ultra-clean exponential laminar flow mobile screen with the turbulent/mixing ventilation system of a small operating room (50m^3) during standardized operations for groin hernia. The presence of the MLAF reduces the mean count of sedimenting bacteria on the patient's chest and the mean air count of bacteria over the patient's chest. The sedimentation rate of bacteria in the periphery of the OR is not significantly affected.

The purpose of the present study is to suggest a possible methodology for assessing the performance of a portable ultra-clean airflow unit by simulating the flow field and dispersion of bacteria-carrying particles within an OR equipped with a vertical laminar airflow system. Different ventilation rates are considered. We aim to investigate the capability of the MLAF to maintain the sterile condition of the instrumentation table and the simultaneous interaction of the device with the general ventilation system, evidenced by the onset of local areas of augmented bacterial contamination within the OR.

2. Materials and methods

2.1. Experimental set-up

The considered prototype of the operating room, shown in Fig. 1, has the horizontal dimensions of 7.0 m × 6.5 m, with a height of 3.0 m. The OR is rigged with essential medical equipment: a surgical table in the center of the room, a multi-purpose column hanging from the ceiling, an anesthesia machine, two scialytic lights suspended above the surgical table using jointed arms, a small movable table, and the principal instrumentation table. The walls are smooth and do not have radiators or windows. The main illumination system consists of strip lights, which are integrated into the ceiling. The medical staff is composed of four surgeons, an anesthesiologist, and an instrumentation nurse. A patient lies on the surgical table.

The main ventilation system complies with the following prescriptions of the international standard ISO 14644: the air change rate is not lower than 15 ACH, the temperature of the supplied air is above 20 °C in winter and below 24 °C in summer (see also ([20])), the concentration of microbes in the inlet air must be lower than one colony-forming-unit (CFU) per cubic meter. The considered air change rates of 15 ACH, 42 ACH and 69 ACH are suitable for clean rooms of ISO 8 and ISO 7 class, respectively. Air recirculation is not allowed (see, e.g. Ref. [20]). Four air supply vents (represented in blue in Fig. 1) open in the upper part of two opposite walls, and four exhaust air vents (represented in red in Fig. 1) are located at floor level, vertically aligned with the inlet vents. Each vent has dimensions (width × height) of 1.16 m × 0.32 m. A vertical-flow, perforated LAF diffuser opens on the ceiling, right above the operating table.

The LAF and each lateral vent supply 0.38 kg/s and 0.077 kg/ s of air for the 15 ACH case, respectively and proportionally higher flow rates for the 42 ACH and 69 ACH ventilation conditions. The surface area of the considered LAF diffuser is 7.74 m^2; the resulting *ceiling coverage* of less than 17% is suitable for operating rooms of class ISO $\geq$ 7. The temperature of the supplied air is 20 °C.

The MLAF unit is modelled as a 0.6 m × 0.65 m × 1.5 m cabinet and positioned near the instrumentation table. It supplies a sterile air-stream of 0.15 kg/s (3 ACH) just above the instrumentation table, with an exit velocity of 0.62 m/s. It is equipped with three suction grills and three supply vents (shown in blue color in Fig. 1), each of width 0.45 m and height 0.15 m. The suction vents are located near the floor, where a higher concentration of BCPs is expected, considering the flow field configuration and the natural tendency of BCPs to settle down.

The main lighting system, the scialytic lights, the staff personnel, the patient, and the powered medical equipment release heat into the surrounding air; the ensuing buoyancy forces affect the flow field and the movement of skin flakes. The heat flux from each source is set according to Brohus et al. [21] and reported in Table 1.

Table 1
Heat flux from occupants and medical equipment.

Heat source	Heat flux [W/m^2]
Surgeon	33.6
Assistant surgeon (each)	26.8
Nurse	28.1
Patient	17.5
Anaesthesiologist	21.1
Scialytic lights (each)	480.0
General illumination	112.5
Anesthesia machine	29.7
Multi-purpose column	78.1

Each individual bacteria-carrying particle (BCP) is potentially a *colony-forming unit* (CFU) [22], as it may give rise to a colony of bacteria under specific conditions of nutrient medium concentration, temperature, and time. Using the CFUs as a measure of the bacterial load is questionable, as some viable bacteria may be unable to grow on culture plates [8,23]. In the present investigation, the bacterial load is estimated by *counting* the concentration of suspended and deposited BCPs; thus, any airborne particle is considered to be bearing a number of viable and potentially dangerous bacteria. Previous studies reported that the size of bacteria-carrying skin scales is distributed in the range 4 μm $-$ $-$ 60 μm, with an average size of 12 μm [24–26]; in the present simulations the BCPs are considered as spherical particles with uniform diameters of 1, 5, or 12 μm and a density of 2 g/cm^3 [11,21,27,28]. The release rate of BCPs is set at 600 CFU/min/person for each member of the medical staff and 400 CFU/min/person for the patient [27].

2.2. Physical and numerical model

The indoor air is modelled as a Newtonian fluid. The thermo-physical properties of air at 20 °C are: $\rho_f = 1.20$ kg/m^3, $c_{p_f} = 1006$ J/kg K, $k_f = 0.0256$ W/m K, $\mu_f = 1.82 \times 10^{-5}$ kg/m s, and $\beta_f = 0.00341$ K^{-1}. The buoyancy force is modelled by the Boussinesq approximation [29]. The Reynolds-Averaged Navier-Stokes (RANS) and energy equations [30] are solved with the commercial model ANSYS® Fluent® v.18.1.0. The realizable $k-\varepsilon$ model [31] has been successfully applied in indoor air simulations [18,32–35]. It is computationally less demanding than Reynolds Stress models, although it provides *realizable* turbulent flow fields, whose state lies within Lumley's triangle (see, e.g., Pope [36, p.393]). A thorough validation of the realizable $k-\varepsilon$ model adopted in the present study is reported in section 2.4.

The surface-to-surface (S2S) model is adopted for thermal radiation, with the assumption of diffuse gray surfaces. The inflow and outflow boundaries are considered to be blackbodies, while the emissivity of the solid walls is taken as 0.9. Additional details on the relevance of thermal radiation for the considered experimental setup are provided in the Supplementary Material.

The Discrete Phase Model (DPM) [37] is used to track the BCPs, which do not interact with each other and do not affect the airflow. Exhaustive details about the adopted DPM model are provided in the accompanying Supplementary Material.

The following boundary conditions are enforced:

- SOLID SURFACES
  - *Airflow*: no-slip boundary condition with standard wall functions
  - *Heat transfer*: either adiabatic surface (room enclosure) or heat-flux condition (staff, electrical equipment)
  - *Radiation*: *gray* surfaces with emissivity 0.9
  - *DPM*: *reflect* boundary condition with variable restitution coefficient (see Table 4) and constant, uniform release rate from the staff with a normal velocity of 0.01 m/s
- INFLOW BOUNDARIES

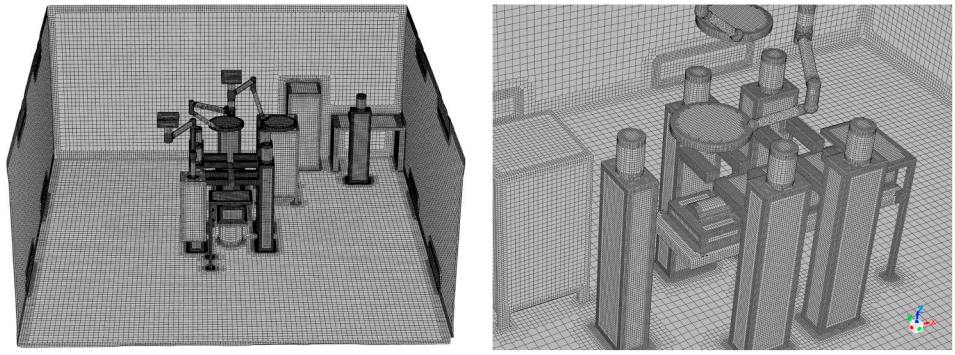

Fig. 2. Different views of the computational mesh C.

Table 2
Mesh-convergence study. y^+ denotes the wall-normal distance from the closest cell center in wall-units. The cell size is defined as the cubic root of the cell volume. τ_w is the (surface-averaged) wall shear stress acting on the top surface of the instrumentation table. h denotes the (surface-averaged) heat transfer coefficient on the instrumentation nurse.

Mesh	Nr cells	y^+ (min, max)	Cell size [m] (min, max)	τ_w [10^{-4} Pa]	h [W/m^2 K]
A	526577	0.04, 142.4	0.0032, 0.14	5.7	6.9
B	921014	0.06, 128.2	0.0030, 0.11	7.5	7.3
C	1889699	0.047, 93.4	0.0023,0.083	7.9	7.9
D	3526347	0.042, 68.9	0.00083, 0.041	8.0	8.0

  - *Airflow*: mass flow-inlet, with different turbulence intensity (0% for the vertical LAF diffuser, 10% for lateral vents and MLAF diffuser)
  - *Heat transfer*: constant, uniform air temperature
  - *Radiation*: blackbody
  - *DPM*: *reflect* boundary condition with restitution coefficient 1.0 and zero release rate, except for the lateral inlet vents during off-design operation (see section 3.3)
- OUTFLOW BOUNDARIES
  - *Airflow and heat transfer*: pressure-outlet condition
  - *Radiation*: blackbody
  - *DPM*: *escape* condition

2.2.1. Computational mesh

A polyhedral computational mesh is generated by *SnappyHexMesh* (Fig. 2), the split-hex mesh generator toolbox of the OpenFOAM® simulation package [38]. Results of a mesh-convergence study are summarized in Table 2; mesh C is used throughout the reported investigation, as it provides a reasonable compromise between accuracy and computational efficiency.

2.3. Limitations of the proposed model

The proposed simplified model does not account for several features of a real operating room:

- The doors of the OR do not open; hence, the considered OR is a closed system, not interacting with a pre-operatory room.
- The staff personnel are standing perfectly still.
- The air in the OR is assumed to be dry.
- The convection of BCPs is modelled; the fate of the bacteria they are carrying, that is, whether they die or grow, is not addressed.
- A single ventilation system is investigated.
- The configuration of the MLAF device is highly simplistic.

2.4. Validation of airflow and DPM models

The numerical model is validated by comparison with the results from Chen et al. [39], who conducted experimental measurements of indoor airflow and particle dispersion within a three-dimensional scale model of a rectangular room, with a transversal section as sketched in Fig. 3. The airflow is directed from a single inlet vent (uniform inlet velocity of 0.225m/s) to a single outlet vent. Silver-coated, hollow glass spheres enter the room with the airflow; their apparent density is 1400 kg/m^3, and their nominal diameter is in the range of 2 μm – 20 μm. Chen et al. [39] measured the airflow velocity and the particle concentration with a phase-Doppler anemometry system, capable of resolving both the diameter and velocity of the particles.

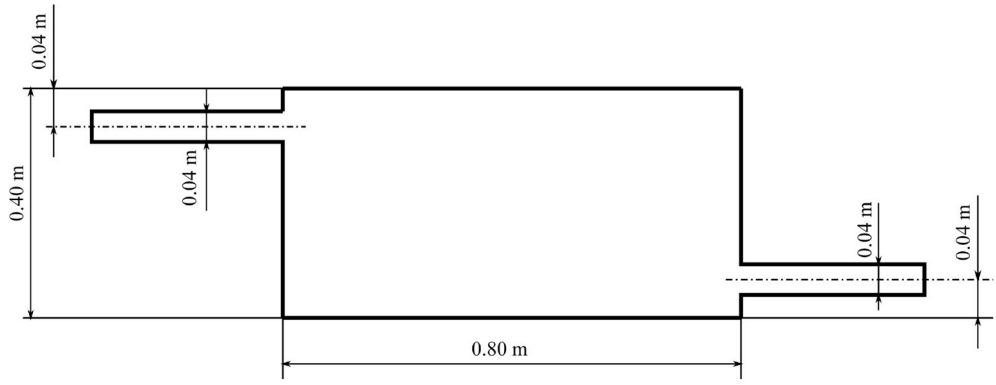

Fig. 3. Sketch of the test room used by Ref. [39].

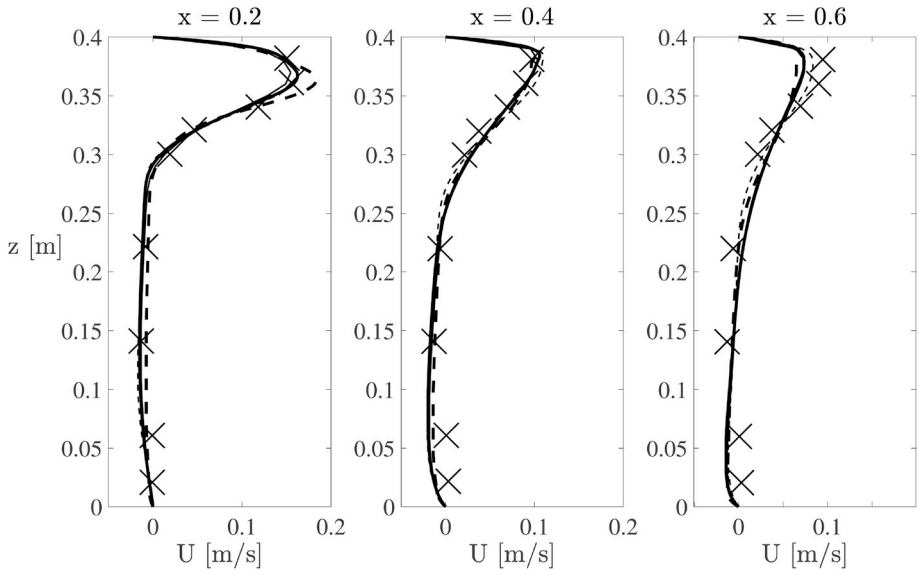

Fig. 4. Vertical profiles of x-velocity. Symbols: experimental measurements by Chen et al. [39]. Solid lines: thin - $k-\varepsilon$ model, thick - $k-\varepsilon$-RNG. Dashed lines: thin - $k-\varepsilon$-Realizable model, thick - RSM model.

Table 3
L_2 error norm of horizontal velocity, scaled by the corresponding norm for the experimental velocity profiles.

Model	Standard $k-\varepsilon$	Realizable $k-\varepsilon$	RNG $k-\varepsilon$	RSM
L_2 error norm (%)	7.7	7.4	8.2	8.0

The airflow distribution within the test room is simulated using different turbulence models. In Fig. 4, the horizontal velocity profile along three equidistant vertical lines is compared against the experimental measurements reported in Ref. [39]. Among the considered turbulence models, the realizable $k-\varepsilon$ model attains the best results for the L_2 error norm, as reported in Table 3.

The DPM model used in the present study is validated by comparing the calculated particle concentration with the experimental data reported by Chen et al [39]. Solid particles with diameters of 10 μm are traced. At the inflow boundaries, the particles move with the airflow. At the outflow boundaries, the particles leave the computational domain. The particles are assumed to create an impact against the solid walls with a prescribed restitution coefficient Ψ:

$$\boldsymbol{u}^{+} = \Psi\left[-\left(\boldsymbol{u}^{-}\cdot\boldsymbol{n}\right)\boldsymbol{n} + \left(\boldsymbol{u}^{-}\cdot\boldsymbol{\tau}\right)\boldsymbol{\tau}\right] \tag{1}$$

The numerical and experimental results for the particle

Table 4
Parameter values chosen as *optimum* for the DPM model.

Parameter	Value
Turb. model	Realizable $k-\varepsilon$
Restit. coeff.	0.5 for arbitrarily-oriented walls 0.0 for horiz. walls facing upwards
C_T	0.1

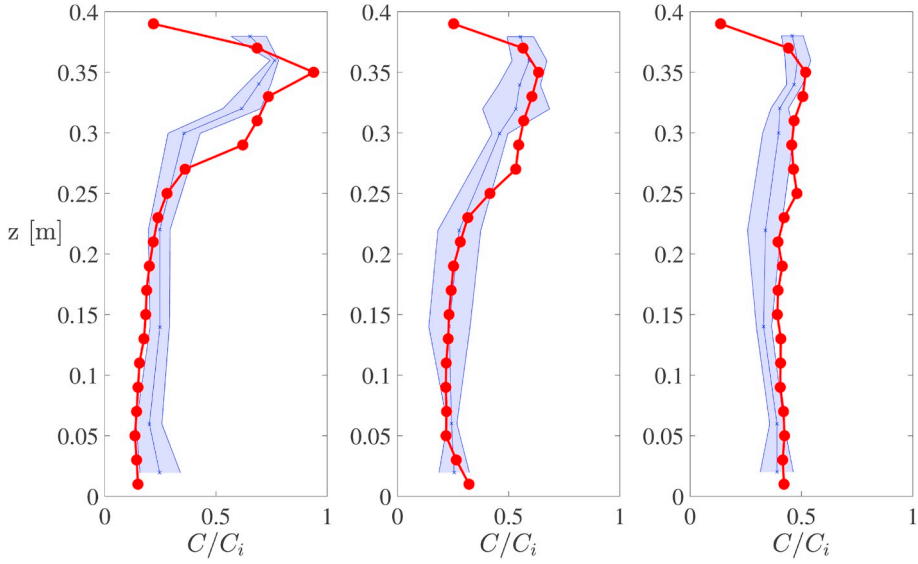

Fig. 5. Comparison of numerical and experimental concentrations along vertical profiles at three longitudinal locations $x = 0.2$ m, $x = 0.4$ m, $x = 0.6$ m on the mid-plane of the room. The error band for the experimental measurements by Chen et al. [39] is reported in light gray. The parameters of the numerical model are reported in Table 4.

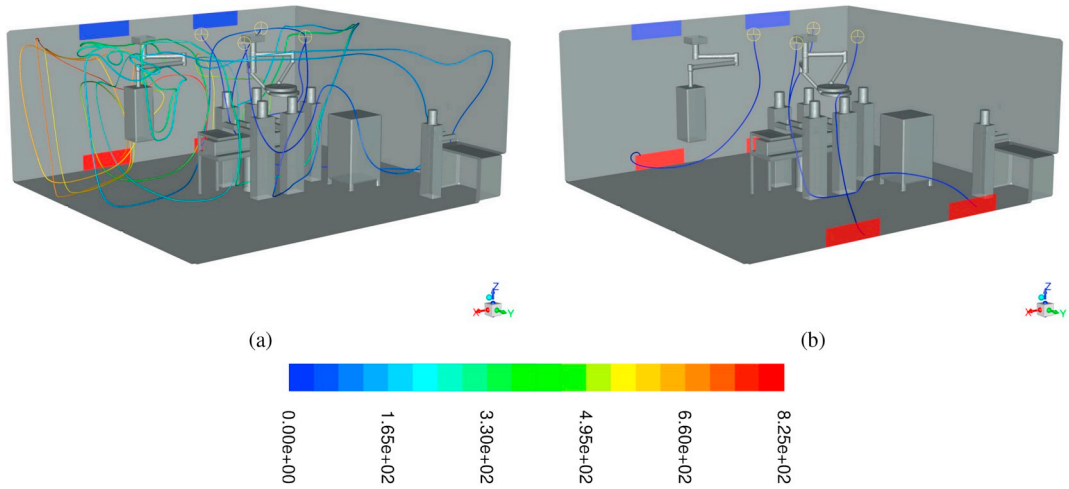

Fig. 6. Streamlines originating from four locations on the LAF, for the two cases without MLAF and ACH = 15 (a), and ACH = 69 (b). The streamlines are colored following the residence time.

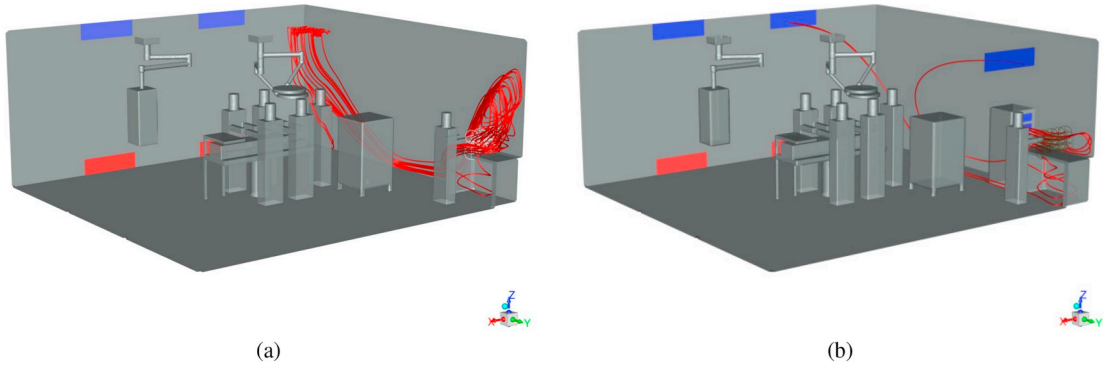

Fig. 7. Back-tracing of some streamlines passing very close above the principal instrumentation table, for the two cases with ACH = 69, without MLAF (a) and with MLAF (b).

concentration on three vertical profiles are compared in Fig. 5. The model options are summarized in Table 4 and used for the simulations of the OR. Different combinations of turbulence models, reflection coefficients for the wall-particle interaction and eddy time-scale parameter C_T (see the Supplementary Material for details) are compared. The best-fitting value found for the time scale constant, $C_T = 0.10$, is lower than the values commonly used with RANS models (0.15 for the $k-\varepsilon$ and 0.30 for the RSM model).

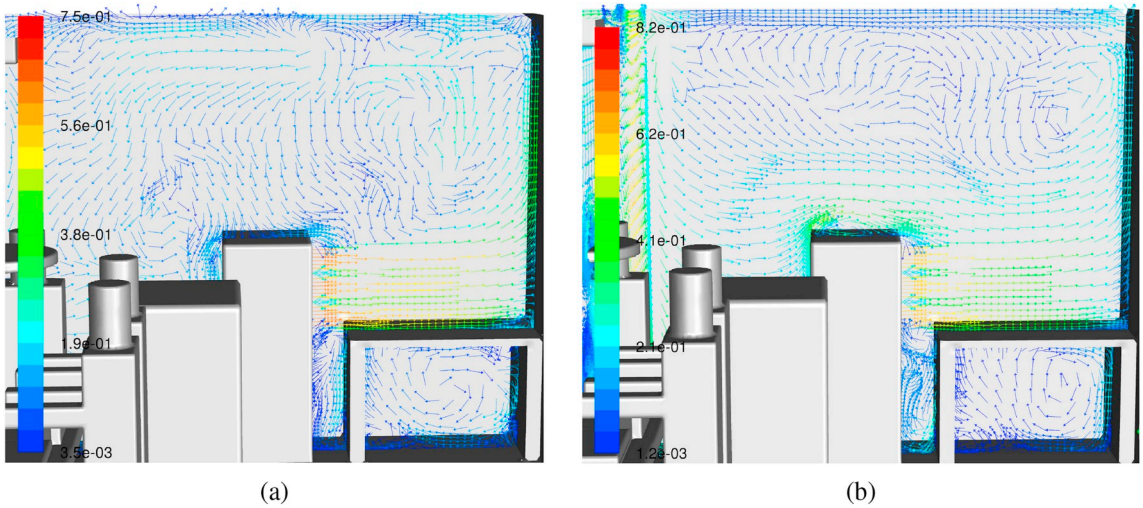

Fig. 8. Projected direction field on a plane. The color represents the velocity magnitude. (a) ACH = 15; (b) ACH = 69. (For interpretation of the references to color in this figure legend, the reader is referred to the Web version of this article.)

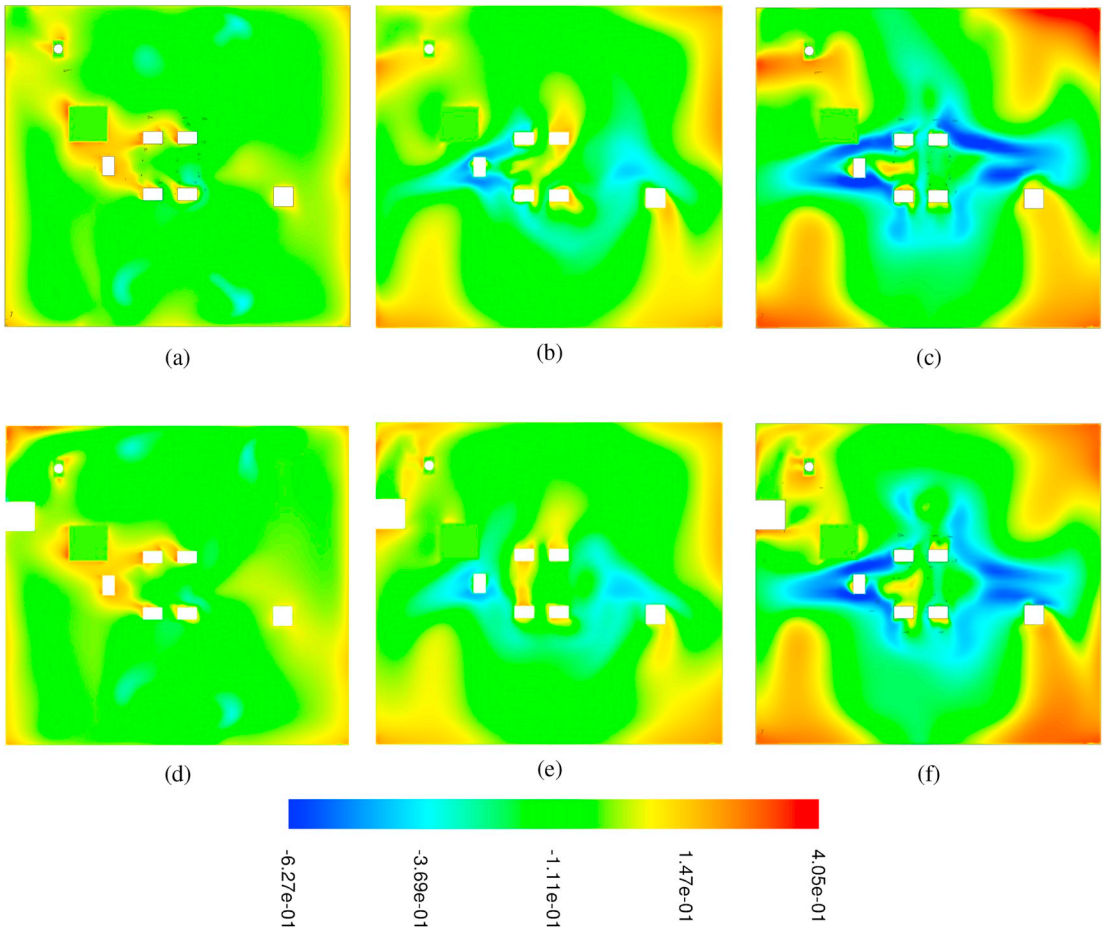

Fig. 9. Contours of vertical velocity on a horizontal plane 1.4 m above the floor, limited to the range [-0.627 m/s, 0.405 m/s]. (a) ACH = 15 without MLAF; (b) ACH = 42 without MLAF; (c) ACH = 69 without MLAF; (d) ACH = 15 with MLAF; (e) ACH = 42 with MLAF (f) ACH = 69 with MLAF.

3. Results and discussion

3.1. Air flow pattern within the OR

The general circulation pattern within the OR can be inferred from the shape of the streamlines released from different vents. Fig. 6 shows streamlines originating from four point-sources on the LAF diffuser for the two cases without MLAF, with ventilation rate of 15 ACH and 69 ACH. With 15 ACH, the streamlines do not show the downward, unidirectional pattern expected for a LAF device; they wobble and form recirculation bubbles. This is caused by the interaction of the airflow with the staff and the furniture. With 69 ACH, the streamlines do not *wander* throughout the OR, but head directly toward the nearest outlet vent. The residence time of fluid particles is considerably reduced, by more than one order of magnitude, in the case of the high ventilation rate. Fig. 7 shows the two cases with the highest ventilation rate. Some streamlines, passing closely above the principal instrumentation table, are back-traced along their way to their corresponding origins. Fig. 7a refers to the case without MLAF, in which some streamlines, originating from an inlet vent, pass above and close to the principal instrumentation table after traveling throughout the operating theater (residence time up to 13 min) and pose a potential risk of bacterial contamination. Fig. 7b refers to the case with MLAF, in which the streamlines passing above the principal instrumentation table originate mostly from the supply vents of the MLAF, whose sterile airflow *shields* the top plane of the instrumentation table.

Fig. 8 shows the projected direction field on a vertical symmetry-plane of the instrumentation table for the cases with MLAF and with (a) ACH = 15 and (b) ACH = 69. Two recirculation regions are noticeable: one below the instrumentation table and the other between the table itself and the MLAF. The airflow supplied by the MLAF entrains the surrounding air and creates a flow recirculation region above the instrumentation table. The entrainment of the surrounding air could possibly be reduced by using *exponential* MLAF screens [13].

Fig. 9 shows the contours of vertical velocity on a horizontal plane 1.4 m above the floor. In all the considered cases, the downward airflow from the LAF is impaired by the presence of obstacles: wakes detach from the medical staff, the anesthesia machine, and the multi-purpose column. Zones of relatively intense updraughts are observed in the main surgical area with low ventilation rate (15 ACH). These are progressively weakened with the increasing downward airflow supplied by the laminar air diffuser. Regions of relatively intense negative vertical velocity develop around the operating theater when the ventilation rate is increased to 42 ACH and 69 ACH. The perturbation induced by the airflow issued by the MLAF has a marginal impact on the distribution of the vertical velocity 1.4 m above the floor, except near and above the principal instrumentation table. The local changes in the airflow pattern within the surgical area, induced by the MLAF, might nevertheless cause significant differences in the sampled concentration of BCPs in that region, where most of the sources of BCPs are concentrated (see section 3.2.3).

3.2. Particle distribution

3.2.1. Air and surface cleanliness classification

The particle deposition rate (PDR) and the air concentration of BCPs depend on several factors such as location, orientation and geometrical configuration of the considered target surface, type of operation,

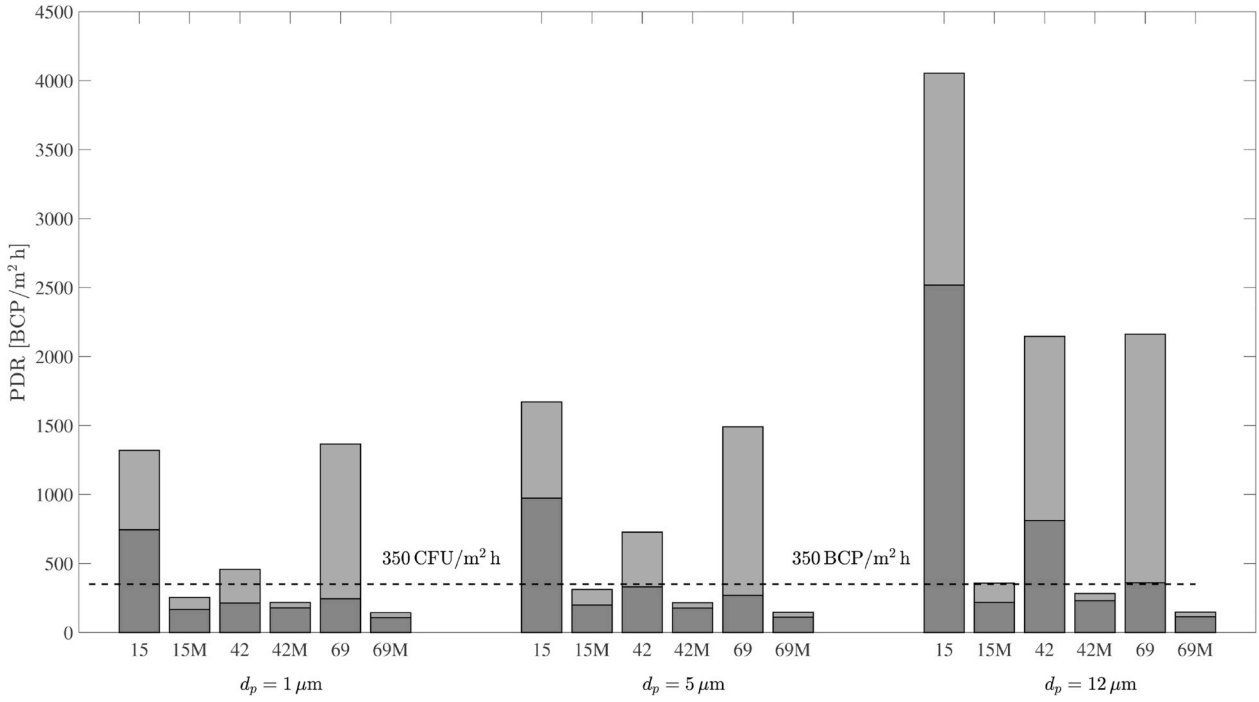

Fig. 10. PDR on the top surface of the instrumentation table. Light-gray bar segments correspond to the contribution to PDR from the instrumentation nurse, while dark-gray bar segments represent the contribution from all other BCP sources. Acronyms 15, 15 M, 69, 69 M indicate the cases 15ACH, 15ACH with MLAF, 69ACH and 69ACH with MLAF, respectively.

Table 5
PDR on principal instrumentation table, for all ventilation rates and all particle diameters. $PDR^{(1)}$ denotes the PDR due to BCPs originated from all sources. $PDR^{(2)}$ denotes the PDR due to BCPs coming from the nurse. $\delta PDR^{(1)}$ accounts for the percent reduction of PDR with respect to the case with the same ventilation rate and the same particle diameter, e.g., case 42 ACH with $d_p = 1\,\mu$m is compared with case 42 ACH with $d_p = 1\,\mu$m and with MLAF. $\delta PDR^{(2)}$ accounts for the percent reduction of PDR with respect to the case with 15 ACH, without MLAF and the same particle diameter, e.g., case 42 ACH with $d_p = 1\,\mu$m is compared with case 15 ACH without MLAF and with $d_p = 1\,\mu$m.

CASE	$d_p[\mu m]$	$PDR^{(1)}$	$PDR^{(2)}$	$\delta PDR^{(1)}$ (%)	$\delta PDR^{(2)}$ (%)
15 ACH	1	1320.0	575.7		
15 ACH	5	1671.0	697.5		
15 ACH	12	4054.0	1536.0		
15 ACH + MLAF	1	254.1	88.3	80.8	80.8
15 ACH + MLAF	5	310.7	112.0	81.4	81.4
15 ACH + MLAF	12	357.3	138.9	91.2	91.2
42 ACH	1	456.9	244.4		65.4
42 ACH	5	727.0	397.0		56.5
42 ACH	12	2146.3	1334.6		47.1
42 ACH + MLAF	1	217.3	39.7	52.4	83.5
42 ACH + MLAF	5	215.2	39.2	70.4	87.1
42 ACH + MLAF	12	282.3	51.8	86.8	93.0
69 ACH	1	1366.0	1122.3		−3.5
69 ACH	5	1491.0	1222.1		10.8
69 ACH	12	2162.0	1801.7		46.7
69 ACH + MLAF	1	142.3	35.1	89.6	89.2
69 ACH + MLAF	5	145.7	35.2	90.2	91.3
69 ACH + MLAF	12	146.6	32.5	93.2	96.4

arrangement of the OR, ventilation setup, and adopted surgical clothing. Based on experiments, conducted in operating rooms equipped with ultra clean vertical or horizontal LAF ventilation, the upper limits of bacterial contamination on surfaces and bacterial concentration in the air are proposed as < 350 CFU/h m^2 and < 10 CFU/m^3, respectively [40,41].

3.2.2. *Deposition rate on the instrumentation table*

The PDR on the top surface of the instrumentation table, at regime conditions, is reported in Fig. 10. The overall cleaning effect of the MLAF is significant for all ventilation rates and for all diameters. As for BCPs of 1 μm and 5 μm, low values of PDR - though higher than the suggested limit - are attained even without the MLAF with the ventilation rate of 42 ACH. When the MLAF is not present, the contribution to the PDR ascribed to the nurse (light gray bar segments in Fig. 10) increases with the ventilation rate, while the contribution of other staff members (dark gray bar segments in Fig. 10) is considerably reduced. The airflow supplied from the MLAF is particularly effective in intercepting the BCPs emitted from the nurse; this *shielding* effect is more evident with the highest considered ventilation rate, when the contribution of the nurse to the PDR drops from $\simeq 82\%$ to $\simeq 23\%$. With the operation of the MLAF, the suggested limit of PDR < 350 particles/h m^2 is attained (or nearly so) by BCPs of any diameter and for all ventilation rates. Table 5 summarizes the reduction of PDR caused by the MLAF for BCPs of different diameters and all considered ventilation rates. Results reported in the fifth column of the table show that the cleaning efficiency of the MLAF increases with d_p while it is non-monotonic with ACH. Results reported in the sixth column provide evidence that increasing the ventilation rate might have controversial effects on the PDR over the instrumentation table and generally does not compensate for the lack of the MLAF device.

3.2.3. *Air concentration of BCPs*

The concentration of BCPs in the air is measured within two spherical control volumes of radius 0.25 m, identified as CV_1 and CV_2. CV_1 is located above the instrumentation table, and CV_2 is positioned above the surgical table (see Fig. 1). Both control volumes are located at a height of 1.5 m above the floor. The number density N (number of particles/m^3) within the considered sampling volumes is reported in Fig. 11.

Increasing the ventilation rate from 15 ACH to 69 ACH induces a decrement of N within both CV_1 and CV_2 for particles of any considered diameter. Increasing the ventilation rate from 15 ACH to 42 ACH, the

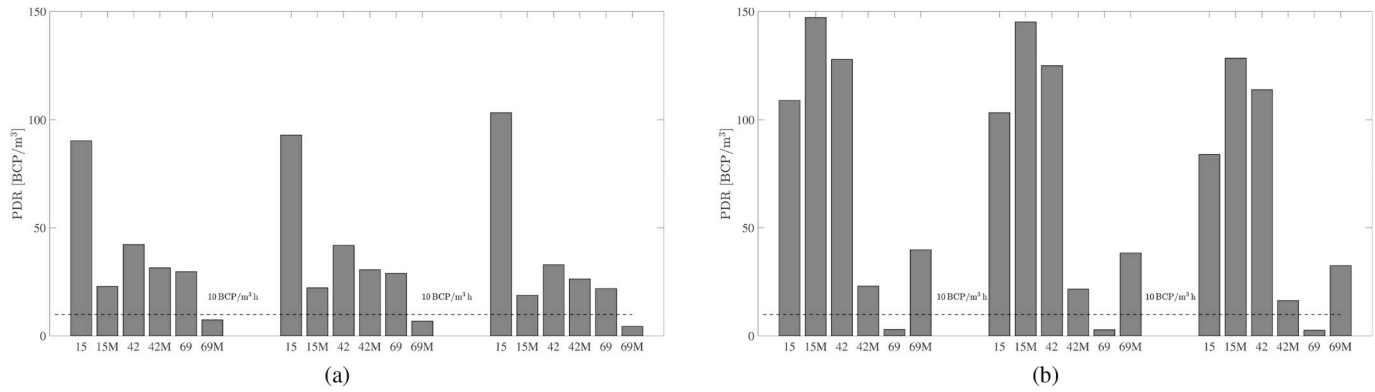

Fig. 11. BCP concentration within two different control volumes for the considered cases and diameters. CV_1 (a); CV_2 (b). Acronyms 15, 15 M, 69, 69 M indicate the cases 15ACH, 15ACH with MLAF, 69ACH and 69ACH with MLAF, respectively.

trend in the change of BCP concentration is independent of the particle diameter while it is different for CV_1 and CV_2 and for cases with or without MLAF. As pointed out in section 3.1, local flow features arising when increasing the ventilation rate in regions of BCP release (e.g., near the nurse and within the surgical area) may result in unexpected high or low BCP concentrations in the selected sampling volumes. Operating the MLAF reduces N within CV_1 with all ventilation rates, while increasing N within CV_2 with 15 ACH and 69 ACH. For the intermediate case with 42 ACH, operating the MLAF causes a reduction of BCP concentration within CV_2 as well. Comparing figures 9b and 9e, it is noticed that an updraught flowing over the surgical table (i.e. across the sampling volume CV_2) when the MLAF is absent disappears when the MLAF is operating. This result is of major relevance as it sheds light on the interference between the clean airflow issued by the MLAF and the general ventilation pattern, which might result in a higher concentration of BCPs in critical regions of the OR. It is noteworthy that the increase in BCP concentration within CV_2 is remarkably more pronounced when the ventilation rate is most intense (69 ACH).

Fig. 12 shows the distribution of the particle number density N on a horizontal plane located 0.5 m above the floor for BCPs of diameter 12 μm and for the extreme ventilation rates 15 ACH and 69 ACH. When the MLAF is not present, increasing the ventilation rate causes a significant reduction in N throughout the OR, even in the recirculation region located under the instrumentation table, where N attains values as high as $\simeq$ 90 BCP/m^3 and $\simeq$ 60 BCP/m^3 in the cases of 15 ACH and 69 ACH, respectively. With both ventilation rates, N attains lower values in the aforementioned recirculation region when the MLAF is active. The MLAF significantly reduces the overall BCP concentration throughout the OR for ACH = 15, while the additional *wash-out* effect is marginal for ACH = 69. Moreover, with the higher ventilation rate, the presence of MLAF significantly widens the region of high BCP concentration (>100 BCP/m^3) in the wake of the four surgeons. Similar considerations hold for particles with $d_p = 1\ \mu$m and $d_p = 5\ \mu$m (figures not reported for brevity).

3.3. Numerical experiments under off-design conditions

The ventilation system for operating rooms must be equipped with high-efficiency particulate air filters (HEPA), capable of reducing the bacterial concentration in the supplied airflow below 1 BCP/ m^3. The theoretical efficiency of HEPA filters is 99.99% for particles with diameter larger than approximately 0.3 μm [42]. However, the actual efficiency of HEPA filters can be lower due to insufficient maintenance, mechanical damage, or accumulation of airborne particulates. The contamination of the instrumentation table is estimated under such *off-design* conditions, with a ventilation rate of 69 ACH. Assuming a statistically-steady airflow throughout the OR, the particle concentration and the PDR under off-design conditions are linearly dependent on the particle emission rate from the inlet vents:

$$N = N_0 + \gamma' \dot{N} \quad \left[BCP / m^3\right] \tag{2}$$

$$PDR = PDR_0 + \gamma'' \dot{N} \quad \left[BCP / \left(m^2\ h\right)\right] \tag{3}$$

where:

- N_0 [BCP/m^3] is the particle concentration under design conditions (i.e., particle emission from the staff only)
- PDR_0 [BCP/(m^2 h)] is the particle deposition rate on the instrumentation table under design conditions (i.e., particle emission from the staff only)
- $\dot{N}$ [BCP/h] is the total emission rate from the lateral supply vents
- γ' [m^{-3} h] and γ'' [m^{-2}] are proportionality coefficients.

The coefficients γ' and γ'' correspond to the increase in BCP and in PDR, respectively, per unit increase in BCP emission rate from the main ventilation system. The calculated values of γ' corresponding to the control volumes CV_1 and CV_2 are listed in Tables 6 and 7, respectively. The calculated values of γ'' are listed in Table 8. The percent difference in γ' and γ'', with respect to the corresponding reference values calculated for the case ACH = 69 and $d_p = 1\ \mu$m, are reported in brackets.

The results reported in Table 6 suggest that the MLAF reduces the contamination of the region above the instrumentation table caused by particles emitted from the lateral vents. This feature is progressively more pronounced for larger particles. The data reported in Table 7 confirm the dramatic increase in BCP concentration above the surgical table caused by the modified airflow circulation induced by the MLAF. As for CV_2, a clear trend for the dependence of γ' on the particle size can not be recognized. With reference to Table 8, γ'' is remarkably reduced when the MLAF is operated; the drop in PDR for particles coming from the lateral vents progressively increases with particle diameters.

4. Conclusions

Movable ultra-clean LAF units provide a viable solution to limit the bacterial contamination in operating rooms. Several authors provide evidence that such devices significantly improve the sterility of specific *targets*, e.g., the surgical table or the instrument table [12,14,19,43]. The airflow supplied from the unit must be intense enough to form a stable, protecting layer of sterile air over these targets. The aforementioned promising results could induce an underestimation of the degree of interaction of movable air cleaners with the existing ventilation patterns within ORs.

The major outcome of the present work is indeed a quantitative determination of such interaction for a model of an OR, where a mobile

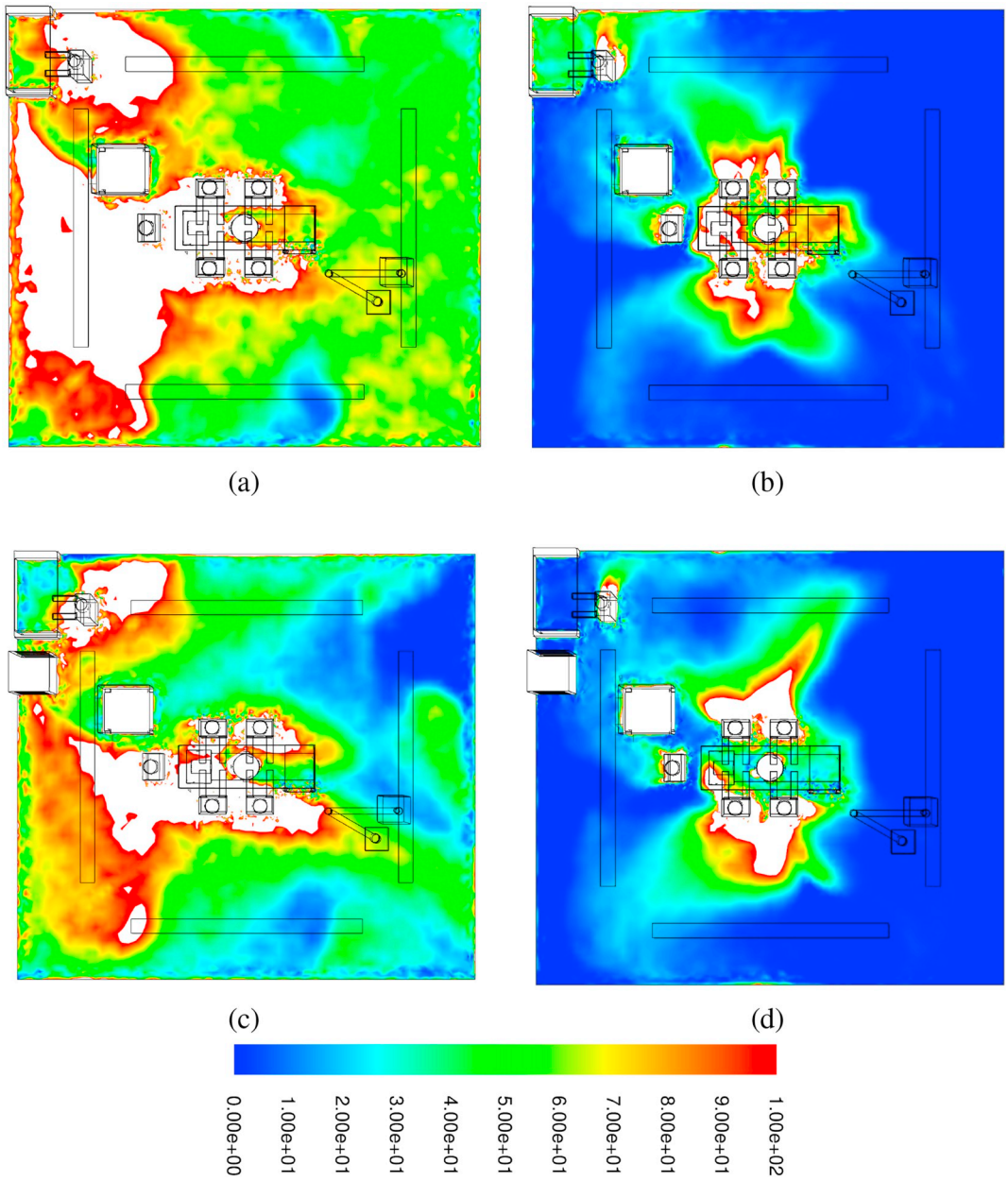

Fig. 12. 12 μm particle concentration (BCP/m^3) on a horizontal plane at z = 0.5 m above the floor, at regime conditions. (a) ACH = 15 without MLAF; (b) ACH = 69 without MLAF; (c) ACH = 15 with MLAF; (d) ACH = 69 with MLAF. White regions correspond either to plane sections of solid bodies (personnel, appliances, furniture) or to areas with particle concentration above 100 BCP/m^3.

Table 6
Coefficients N_0 and γ' for air particle concentration in CV_1, see equation (2).

d_p [μ m]	Coefficients	69 ACH	69 ACH - MLAF
1	N_0 [BCP/m^3]	29.7	7.50
	γ' [$\times 10^{-4}$ m^{-3} h]	1.24 (0%)	1.14 (−8.1%)
5	N_0 [BCP/m^3]	29.0	6.90
	γ' [$\times 10^{-4}$ m^{-3} h]	1.21 (−2.4%)	1.06 (−14.5%)
12	N_0 [BCP/m^3]	21.9	4.30
	γ' [$\times 10^{-4}$ m^{-3} h]	1.14 (−8.1%)	0.75 (−39.5%)

Table 7
Coefficients N_0 and γ' for air particle concentration in CV_2, see equation (2).

d_p [μ m]	Coefficients	69 ACH	69 ACH - MLAF
1	N_0 [BCP/m^3]	2.90	39.8
	γ' [$\times 10^{-5}$ m^{-3} h]	0.106 (0%)	2.01 (+1796%)
5	N_0 [BCP/m^3]	2.80	38.3
	γ' [$\times 10^{-5}$ m^{-3} h]	0.106 (0%)	2.01 (+1796%)
12	N_0 [BCP/m^3]	2.60	32.5
	γ' [$\times 10^{-5}$ m^{-3} h]	0.128 (+20.8%)	1.84 (+1636%)

air-cleaner provides a sterile airflow over the principal instrumentation table although, at the same time, altering the circulation pattern within the OR, in particular within the main surgical area. The interior design of the room and its connection with the pre-operatory area, the number and activity of the OR staff, the intensity of ventilation, the dimension of the airborne particles affect the particle deposition rate on different

Table 8
Coefficients PDR_0 and γ'' for particle deposition rate on the instrumentation table, see equation (3).

d_p [μ m]	Coefficients	69 ACH	69 ACH - MLAF
1	PDR_0 [BCP/(m^2 h)]	1370	142
	γ'' [$\times 10^{-3}$ m^{-2}]	1.03 (0%)	0.466 (−54.8%)
5	PDR_0 [BCP/(m^2 h)]	1490	146
	γ'' [$\times 10^{-3}$ m^{-2}]	1.47 (+42.7%)	0.525 (−49.0%)
12	PDR_0 [BCP/(m^2 h)]	2160	147
	γ'' [$\times 10^{-3}$ m^{-2}]	3.69 (+258%)	0.882 (−14.4%)

surfaces and the particle concentration in air throughout the room. In the present investigation, a single arrangement of the OR is considered and the staff personnel is still. Three ventilation conditions are taken into account: 15 ACH, 42 ACH and 69 ACH of sterile air are supplied from the laminar airflow unit and from four lateral vents. Airborne particles of 1, 5 and 12 μm are tracked.

The sterile airflow from the movable air cleaner significantly reduces the contamination on and over the instrumentation table, by intercepting the stream of BCPs released from the instrumentation nurse. This effect is more relevant for the two extreme ventilation conditions, as the ventilation of 42 ACH provides a low PDR for small BCPs (1 and 5 μm) even without the MLAF. The bacterial contamination of the surgical area, enclosing most of the sources of BCPs, is monitored by measuring the concentration of BCPs within a sampling volume (CV_2) located just above the surgical table. It turns out that this concentration is strongly dependent on the local flow features, which in turn are affected by the airflow supplied by the MLAF: for the ventilation rate of 15 ACH the concentration of BCPs within CV_2 increases only marginally, while with 69 ACH it rises by an order of magnitude. The intermediate ventilation condition, 42 ACH, shows an opposite trend: a local airstream carrying the BCPs directly from the patient towards CV_2 disappears when the MLAF is operating, inducing a remarkable reduction in BCP concentration within CV_2 itself.

The present work provides a possible methodology for evaluating the effective usefulness of an MLAF installation within a specific OR and a reliable estimate of its cleaning efficiency, complementing previous analyses on the effectiveness of movable ultra-clean air cleaners in operating rooms; the variability of geometry, flow conditions, and normal practice of the surgical staff in different operating rooms prevents any general conclusions about this issue and any case should be treated independently. This is more a matter of fact than an inherent limitation of the reported investigation, as the surgical area is both a critical target zone and a zone of major release of BCPs: the modification of the local flow circulation pattern in that area, caused by the airflow supplied from the MLAF, is unpredictable a-priori and may result in a significant deterioration of the sterility of the area, under certain flow conditions. More pragmatically, it is highly risky to simply endow a movable ultra-clean air cleaner in an existing OR without verifying the impact of this action on the bacterial contamination throughout the entire OR under the different *working conditions* of the OR itself.

Funding sources

This research did not receive any specific grant from funding agencies in the public, commercial, or not-for-profit sectors.

Declaration of competing interest

None.

Appendix A. Supplementary data

Supplementary data to this article can be found online at https://doi.org/10.1016/j.buildenv.2020.106643.

References

[1] S. Dharan, D. Pittet, Environmental controls in operating theatres, J. Hosp. Infect. 51 (2) (2002) 79–84.
[2] O.M. Lidwell, E.J.L. Lowbury, W. Whyte, R. Blowers, S.J. Stanley, D. Lowe, Bacteria isolated from deep joint sepsis after operation for total hip or knee replacement and the sources of the infections with staphylococcus aureus, J. Hosp. Infect. 4 (1) (1983) 19–29.
[3] C.E. Edmiston Jr., G.R. Seabrook, R.A. Cambria, K.R. Brown, B.D. Lewis, J. R. Sommers, C.J. Krepel, P.J. Wilson, S. Sinski, J.B. Towne, Molecular epidemiology of microbial contamination in the operating room environment: is there a risk for infection? Surgery 138 (4) (2005) 573–582.
[4] C.A. Petti, L.L. Sanders, S.L. Trivette, J. Briggs, D.J. Sexton, Postoperative bacteremia secondary to surgical site infection, Clin. Infect. Dis. 34 (3) (2002) 305–308.
[5] F. Memarzadeh, A.P. Manning, Comparison of operating room ventilation systems in the protection of the surgical site, in: ASHRAE TRAN vol. 108, 2002, pp. 3–15. PART 2.
[6] J. Charnley, N. Eftekhar, Postoperative infection in total prosthetic replacement arthroplasty of the hip–joint with special reference to the bacterial content of the air of the operating room, BRIT J SURG 56 (9) (1969) 641–649.
[7] B. Friberg, S. Friberg, L.G. Burman, Correlation between surface and air counts of particles carrying aerobic bacteria in operating rooms with turbulent ventilation: an experimental study, J. Hosp. Infect. 42 (1) (1999) 61–68.
[8] M. Alsved, A. Civilis, P. Ekolind, A. Tammelin, A.E. Andersson, J. Jakobsson, T. Svensson, M. Ramstorp, S. Sadrizadeh, P.-A. Larsson, M. Bohgard, T. Šantl Temkiv, J. Löndahl, Temperature-controlled airflow ventilation in operating rooms compared with laminar airflow and turbulent mixed airflow, J. Hosp. Infect. 98 (2) (2018) 181–190.
[9] O.M. Lidwell, E.J.L. Lowbury, W. Whyte, R. Blowers, S.J. Stanley, D. Lowe, Effect of ultraclean air in operating rooms on deep sepsis in the joint after total hip or knee replacement: a randomised study, BRIT MED J 285 (6334) (1982) 10–14.
[10] C. Brandt, U. Hott, D. Sohr, F. Daschner, P. Gastmeier, H. Rüden, Operating room ventilation with laminar airflow shows no protective effect on the surgical site infection rate in orthopedic and abdominal surgery, Ann. Surg. 248 (5) (2008) 695–700, https://doi.org/10.1097/SLA.0b013e31818b757d.
[11] N. Kamsah, H.M. Kamar, M.I. Alhamid, W.K. Yinn, Impacts of temperature on airborne particles in a hospital operating room, J. Adv. Res.Fluid Mech.Therm. Sci. 44 (1) (2018) 12–23.
[12] K.-G. Nilsson, R. Lundholm, S. Friberg, Assessment of horizontal laminar air flow instrument table for additional ultraclean space during surgery, J. Hosp. Infect. 76 (3) (2010) 243–246.
[13] S. Sadrizadeh, S. Holmberg, Effect of a portable ultra-clean exponential airflow unit on the particle distribution in an operating room, Particuol. 18 (2015) 170–178.
[14] C. Pasquarella, G.E. Sansebastiano, S. Ferretti, E. Saccani, M. Fanti, U. Moscato, G. Giannetti, S. Fornia, P. Cortellini, P. Vitali, C. Signorelli, A mobile laminar airflow unit to reduce air bacterial contamination at surgical area in a conventionally ventilated operating theatre, J. Hosp. Infect. 66 (4) (2007) 313–319.
[15] K. Urashima, J.-S. Chang, Removal of volatile organic compounds from air streams and industrial flue gases by non-thermal plasma technology, IEEE T Dielect el in 7 (5) (2000) 602–614.
[16] S. Gruber, S. Buhl, C. Bulitta, Innovative ventilation technology for operating rooms, Curr. Dir.Biomed. Eng. 4 (1) (2018) 243–245, https://doi.org/10.1515/cdbme-2018-0059.
[17] A.-C. von Vogelsang, P. Förander, M. Arvidsson, P. Löwenhielm, Effect of mobile laminar airflow units on airborne bacterial contamination during neurosurgical procedures, J. Hosp. Infect. 99 (3) (2018) 271–278, https://doi.org/10.1016/j.jhin.2018.03.024.
[18] S. Sadrizadeh, A. Afshari, T. Karimipanah, U. Håkansson, P.V. Nielsen, Numerical simulation of the impact of surgeon posture on airborne particle distribution in a turbulent mixing operating theatre, Build. Environ. 110 (2016) 140–147.
[19] S. Friberg, B. Ardnor, R. Lundholm, B. Friberg, The addition of a mobile ultra-clean exponential laminar airflow screen to conventional operating room ventilation reduces bacterial contamination to operating box levels, J. Hosp. Infect. 55 (2) (2003) 92–97.
[20] C.A. Balaras, E. Dascalaki, A. Gaglia, Hvac and indoor thermal conditions in hospital operating rooms, Energ Buildings 39 (4) (2007) 454–470, https://doi.org/10.1016/j.enbuild.2006.09.004.
[21] H. Brohus, K.D. Balling, D. Jeppesen, Influence of movements on contaminant transport in an operating room, Indoor Air 16 (5) (2006) 356–372.
[22] A. Charkowska, Ensuring cleanliness in operating theatres, Int. J. Occup. Saf. Ergon. 14 (4) (2008) 447–453.
[23] R.I. Amann, W. Ludwig, K.-H. Schleifer, Phylogenetic identification and in situ detection of individual microbial cells without cultivation, Microbiol. Rev. 59 (1) (1995) 143–169.
[24] W.C. Noble, O.M. Lidwell, D. Kingston, The size distribution of airborne particles carrying micro-organisms, J HYG-CAMBRIDGE 61 (4) (1963) 385–391.
[25] W.C. Noble, Dispersal of skin microorganisms, Brit J Dermatol 93 (4) (1975) 477–485.

[26] M. Persson, Airborne contamination and surgical site infection: could a thirty-year-old idea help solve the problem? Med. Hypotheses 132 (2019) https://doi.org/10.1016/j.mehy.2019.109351.
[27] J. Liu, H. Wang, W. Wen, Numerical simulation on a horizontal airflow for airborne particles control in hospital operating room, Build. Environ. 44 (11) (2009) 2284–2289.
[28] J.-L. Poirot, J.-P. Gangneux, A. Fischer, M. Malbernard, S. Challier, N. Laudinet, V. Bergeron, Evaluation of a new mobile system for protecting immune-suppressed patients against airborne contamination, Am J Infect Control 35 (7) (2007) 460–466.
[29] P.K. Kundu, I.M. Cohen, D.R. Dowling, Fluid Mechanics, sixth ed. edition, Academic Press, Boston, MA, 2016.
[30] H. Tennekes, J.L. Lumley, A First Course in Turbulence, MIT Press, 1972.
[31] T.-H. Shih, W.W. Liou, A. Shabbir, Z. Yang, J. Zhu, A new k-εeddy viscosity model for high Reynolds number turbulent flows, *Comput. Fluids* 24 (3) (1995) 227–238.
[32] Q. Chen, Comparison of different k-εmodels for indoor air flow computations, Numer Heat TR B-Fund 28 (3) (1995) 353–369.
[33] K. Van Maele, B. Merci, Application of two buoyancy-modified k-εturbulence models to different types of buoyant plumes, Fire Safety J 41 (2) (2006) 122–138.
[34] Z.J. Zhai, Z. Zhang, W. Zhang, Q.Y. Chen, Evaluation of various turbulence models in predicting airflow and turbulence in enclosed environments by cfd: Part 1—summary of prevalent turbulence models, HVAC R Res. 13 (6) (2007) 853–870.
[35] F. Kuznik, G. Rusaëoun, J. Brau, Experimental and numerical study of a full scale ventilated enclosure: comparison of four two equations closure turbulence models, Build. Environ. 42 (3) (2007) 1043–1053.
[36] B. Stephen, Pope. *Turbulent Flows*, Cambridge University Press, 2000.
[37] J.G.M. Kuerten, Point-particle dns and les of particle-laden turbulent flow - a state-of-the-art review, Flow, Turbul. Combust. 97 (3) (2016) 689–713.
[38] H.C. Weller, G. Tabor, H. Jasak, C. Fureby, A tensorial approach to computational continuum mechanics using object-oriented techniques, Comput. Phys. 12 (6) (1998) 620–631, https://doi.org/10.1063/1.168744.
[39] F. Chen, S.C.M. Yu, A.C.K. Lai, Modeling particle distribution and deposition in indoor environments with a new drift-flux model, Atmos. Environ. 40 (2) (2006), 357–36.
[40] B. Friberg, S. Friberg, L.G. Burman, Inconsistent correlation between aerobic bacterial surface and air counts in operating rooms with ultra clean laminar air flows: proposal of a new bacteriological standard for surface contamination, J. Hosp. Infect. 42 (4) (1999) 287–293.
[41] W. Whyte, O.M. Lidwell, E.J.L. Lowbury, R. Blowers, Suggested bacteriological standards for air in ultraclean operating rooms, J. Hosp. Infect. 4 (2) (1983) 133–139.
[42] T.T. Chow, X.Y. Yang, Performance of ventilation system in a non-standard operating room, Build. Environ. 38 (12) (2003) 1401–1411.
[43] S. Sadrizadeh, S. Holmberg, A. Tammelin, A numerical investigation of vertical and horizontal laminar airflow ventilation in an operating room, Build. Environ. 82 (12 2014) 517–525.